A Three Dimensional Analysis of Frog Gastrulation

Following investigations into the role of calcium signaling during gastrulation in the frog, *Xenopus laevis*, we became interested in a accurately the three dimensional structure of the *Xenopus* gastrula in normal and experimentally manipulated embryos. We developed a surface imaging microscopy (SIM) [1] to accomplish this goal. We have applied SIM to the study of *Xenopus* gastrulation and have recently competed a digital atlas of frog gastrulation, with every substage from blastula through neurula represented.

To take best advantage of these digital volumes, we developed a standard coordinate system for comparing embryos, then developed computational tools to define the surface of the embryos and extract curved surfaces and volumes according to this coordinate system. These computational tools enabled us to make detailed comparison of the same regions within different *Xenopus* embryos. We applied these techniques to visualize the internal events of gastrulation as a function of stage. We have also visualized the vegetal alignment zone, an arrangement of cells in the mesoderm predicted to close the blastopore, but never previously directly visualized in an intact embryo. We then imaged embryos, at two stages of development, that were overexpressing a mutant form of Disheveled in their dorsal mesoderm. These embryos had nearly normal archenteron lengths, but deficient mesodermal convergent extension, implying that the archenteron can elongate in the absence of normal mesodermal cell movements. We conclude by discussing plans to test this hypothesis, and to directly measure the extent of coupling of different morphogenetic processes during gastrulation.

Andrew Ewald, J. Michael Tyszka,

Scott E. Fraser, John Wallingford

Biological Imaging Center

California Institute of Technology

Introduction

My research into the control of cell movements in the *Xenopus* gastrula began by looking for molecular mechanisms for coordinating cell motility in the dorsal mesoderm. We discovered, characterized the tissue specificity of, and demonstrated the requirement for propagating intercellular waves of calcium in the dorsal mesoderm (Chapter 4). We concluded that calcium was required for the elongation of the dorsal mesoderm by examining the elongation of the embryo's developing anterior posterior axis (as revealed by in situ hybridization for a notochord specific molecular marker). The defect was profound and highly penetrant. I was unsatisfied with our ability to fully characterize the full extent of the phenotype though. *Xenopus* embryos are large and highly opaque, making optical analysis of whole embryos quite difficult. Traditional histological methods can be used to prepare thin sections of almost any part of the embryo, but it is very difficult to reconstruct three dimensional volumes accurately from isolated sections. I wanted to be able to interactively visualize whole frog embryos to determine the full nature of defects caused by different molecular disruptions. I wanted to understand what had gone wrong in response to a given perturbation and, just as important, what worked despite the perturbation.

In parallel experiments we were developing surface imaging microscopy as a tool for visualizing large embryo samples at high resolution (Chapter 4). Briefly, we have applied this technique to frog gastrulation, and have used to it visualize the

major events of gastrulation, and to evaluate the phenotype of disruptions in Disheveled signaling.

Results/Discussion

SIM Produces High Resolution Digital Frog Datasets

We have found that SIM is ideally suited to the study of early frog development. Since the magnification of the final images is selected prior to imaging, and the sample is destroyed during imaging, SIM works best with embryos that are of similar size, so that a similar level of detail can be observed in all conditions. We have previously tested SIM on chick, frog, and mouse embryos (Chapter 5). It produced high quality images of all three species, but the extensive growth that is characteristic of early mouse and chick development put practical limits on the developmental window that could be examined. Since early frog development occurs with very little net change in volume, we were able to select a single resolution and image embryos at all stages of gastrulation with equivalent contrast and resolution. We present a quick review of the technique behind SIM in Figure 6-1.

Comparison with Confocal Microscopy

The *Xenopus* embryos is highly opaque and scatters light very effectively. Consequently we have been unable to image more than a 20-30 microns into the surface of a living or fixed frog embryo. The use of Murray's Clearing Solution

minimizes these problems, and reduces scattering sufficiently to enable imaging of whole, intact frog embryos with a confocal microscope [2]. The quality of the individual sections is reasonable, but the resolution is highly anisotropic, making it very difficult to accurately visualize structures except within the original plane of optical section. Figure 6-2A demonstrates the quality of image data that can be achieved in whole embryos that have been cleared and imaged with a confocal microscope. As a contrast we present a typical quality SIM dataset of a late gastrula frog embryo in Figure 6-2B. The contrast and in-plane resolution are at least as good and the through plane resolution is much better. We are not aware of another technique which can image a sample of this size (1-1.2 mm) at this resolution (1.77 um^2).

The one technical feature that we are still working to develop in SIM, that is exceeded in confocal microscopy, is the visualization of specific fluorescent stains. We have used Resolution Standard Stain for all of the embryos in this chapter, and were not successful in imaging green fluorescent protein or labeled antibodies with SIM. This matter is discussed in Chapter 5.

Coordinate System

We have successfully imaged more frog embryos at every stage of frog gastrulation. To facilitate making comparisons between embryos at the same stage to assess the variability of events of gastrulation, or to compare normal embryos with experimentally perturbed embryos, we developed a standard

coordinate system for frog gastrulation. Since the frog gastrula is very nearly spherical, we decided to work in spherical coordinates. To define a spherical coordinate system, it is necessary to select a pole and the prime meridian. Once that is done all other points in the sphere can be uniquely identified. We chose to define the center of the blastopore as the South Pole, and a normal through that point to define the North Pole. We defined the prime meridian as the center of the dorsal lip of the blastopore. We spent some time trying to develop algorithms to automatically identify these landmarks, but it proved very challenging to computationally mimic the trained eye of a developmental biologist. Instead we chose to develop algorithms (described Methods and in Appendix 2) to enable quick manual selection of these landmarks. Figure 6-3 shows screen captures of our blastopore and archenteron selection schemes.

Digital Atlas of Frog Gastrulation

We have successfully imaged approximately 40 frog embryos at different stages of development, covering Nieukoop and Faber stages 9-14 [3]. A selection of these embryos is presented in Figure 6-4. As can be seen clearly in Figure 6-4, the gastrula stage frog embryo is very nearly spherical. The biological organization of the embryo at these stages is chiefly in radially concentric curved surfaces. We have taken advantage of these facts to digitally manipulate these datasets to visualize the major events of frog gastrulation. We computationally identify the sphere which best fits the surface of the embryo (see Appendix 2), then define a coordinate system for the embryo. Once this coordinate system is

selected we can extract any surface or volume from the embryo. Since the coordinate system enables us to compare similar regions in embryos of different stages or different experimental conditions, we can visualize internal events of gastrulation as a function of stage or perturbation.

To illustrate this process, we have selected four embryos from our digital atlas; they are presented in volume renderings in Figure 6-5. For our current purposes we are most interested in the polarity of cells and tissues in the dorsal marginal zone. Much recent work has focused on the molecular control of cell movements in this tissue (reviewed in [4-6]). We wanted to visualize three events in this tissue: tissue separation, bottle cell formation, and archenteron elongation. We have conducted a preliminary analysis and concluded that we have sufficient resolution and contrast to see these events.

Figure 6-6 depicts the two basic volumes that we have extracted from the embryos shown in Figure 6-5. To visualize the dorsal marginal zone we extracted surfaces from the center of the blastopore to the margin of the embryo, from a radius of 0.5 through 0.95 (with 1 being the surface of the best-fit sphere), and from a range of longitudes of +/- 60° from the center or the dorsal lip. We then mapped that volume to a rectangular block for ease of manipulations. We have also explored a variety of cartographic projections, but have yet to find one suitable for conveniently examining volumes. The second volume we extracted was a more superficial peel (radius 0.75-0.95), but ranging in latitude from the

South Pole (center of blastopore) to the North Pole, and ranging in longitude +/- 60° from the center of the dorsal lip of the blastopore.

Evaluation of Diagnostic Ability of Datasets

We have extracted these two volumes from the four embryos presented in Figure 6-5 and have just finished a preliminary evaluation of our computational tools. To determine the utility of these datasets for analyzing the phenotypes experimentally perturbed embryos, we developed techniques to visualize the key diagnostic events of gastrulation. We present examples of several of these below.

Involution and Tissue Separation

Figure 6-7 depicts two of the main events of gastrulation, involution and tissue separation. One of the major functions of gastrulation is to establish the developing gut, or archenteron. The archenteron forms when a group of cells at the dorsal lip of the blastopore restricts their apical surfaces and forms the indentation visible in Figure 6-7A. The gut then advances through the solid tissue of the embryo (black line in 6-7B and 6-7C), and eventually forms a large lumen (Figure 6-7D). Coincident with this process is the separation of different adjacent tissues within the embryo [7, 8], which has been shown to be under the control of Wnt signaling through Frizzled-7 [9]. We can clearly visualize the interface between the separating tissues (black arrows in Figure 6-7) and can

visualize the spatial relationship between this interface and lengthening archenteron.

Vegetal Alignment Zone

Another key event of gastrulation is the closure of the blastopore. This is currently thought to be mechanically achieved through the development of bands of aligned cells in concentric hoops around the blastopore. Mediolateral alignment of cells in this region, consistent with this idea, was observed in the 1970s [10, 11], and bands of aligned cells were observed in explants of these tissues in the early 1990s [12]. Due to technical imaging challenges, these cell rearrangements have not been observed in intact embryos. We examined surfaces in gastrula embryos at the depths indicated in Figure 6-8. When examining the three dimensional volume, and surfaces extracted from that volume, we have found cell alignments consistent with the vegetal alignment zone (Figure 6-8 D-G). We are still testing methods to convincingly visualize this structure.

Mesendoderm Extension

The final structure that we chose to visualize is the leading edge of the mesendoderm. A semi-coherent population of mesoderm and endoderm starts near the floor of the blastocoel and migrates/extends over the surface of the blastocoel roof. We visualized this process in the long, thin embryo volumes and

depict this in Figure 6-9. This process was dynamically imaged in living embryos in a recent report [13], and our observations are consistent with theirs.

Experimental Disruption of Dishevelled Signaling

The process of convergent extension in the dorsal mesoderm of the frog embryo has been shown to be under the control of Wnt signaling through the planar cell polarity pathway [14, 15]. More recent studies have demonstrated a direct role for Dishevelled in the medio-lateral polarity of cells within the dorsal mesoderm [16], reviewed in [4, 5]. Since we demonstrated that our digital frog gastrulation atlas was capable of visualizing the major events of frog gastrulation, we decided to image embryos overexpressing a mutant form of Dishevelled, Xdd1 [17], in the dorsal mesoderm. We imaged control and injected embryos at the beginning (6-10) and end (Figure 6-11) of gastrulation.

The most striking thing about the early gastrula Xdd1 embryos is how normal they look. This time point (Stage 10.5) is prior to most of the major cell movements of gastrulation. Since the major cell movements up to this point involve the deep vegetal cells, which were untreated, this is not too surprising.

The late gastrula embryos have several obvious defects: the archenteron volumes are smaller, the blastocoel volume is larger, and the tissue between the archenteron and the surface of the embryo appears thicker. We were most struck by the fact that the archenteron elongation is fairly normal: the

archenterons are slightly (20%) shorter than control embryos. It is presently unclear how the volume of the archenteron increases and the blastocoel decreases, so we chose to focus on two of these differences: that the length of the archenteron is shorter, and the marginal zone is thicker. These two observations make two testable predictions: that radial intercalation within the dorsal marginal zone is dependent on Dishevelled function in the dorsal marginal zone, and that archenteron elongation is not.

Conclusions

We have applied surface imaging microscopy to the process of frog gastrulation and generated a digital atlas comprising all stages of gastrulation. We have developed a standard coordinate system for these embryos to facilitate comparisons, and have developed computational methods to extract deep surfaces from these datasets. We have just finished a preliminary analysis of the level of detail in this datasets and have concluded that we can observe bottle cell formation, tissue separation, archenteron elongation, blastopore closure, and mesendoderm extension. We also have suggestive evidence that we will be able to visualize the vegetal alignment zone in intact embryos. Finally we have imaged embryos with disruptions in Dishevelled function and have generated two novel testable predictions: that radial intercalation is and archenteron elongation is not dependent on Dishevelled function in the dorsal mesoderm. We have also developed techniques to test these hypotheses.

Future Directions

We will apply the computational methods described in this paper to the comparative analysis of the normal and Xdd1 embryos at both stages. In parallel, we plan to use simpler techniques to test the degree of coupling of archenteron elongation, dorsal mesodermal convergent extension, and blastopore closure in normal and Xdd1 embryos. We will measure the area of the blastopore normalized to the area of the embryo (Figure 6-12a), the length to width ratio of the notochord domain (Figure 6-12b), and then surgically bisect the embryos along the dorsal midline, and measure the length of the archenteron normalized to the diameter of the embryo. It is necessary to make all of the measurements relative to the size of the individual embryo, as early *Xenopus* embryos vary in size significantly. These measurements within normal embryos will give us a precise measure of the degree of coupling of these three processes during normal gastrulation. By also analyzing Xdd1 overexpressing embryos we can get a definite test of the our hypotheses that radial intercalation is affection and archenteron elongation is not.

Materials and Methods

Surface Imaging Microscopy

Frog embryos were prepared and imaged accordingly to protocols developed and reported in Chapter 5.

Best Fit Sphere and Shell Extraction

Appendix 2-14 details our approach to establishing a coordinate system for each dataset and extracting surfaces from those datasets. Figures 6-7 and 6-8 were generated with latitude –90-0, radius 0.5-0.95, longitude –60-60. Figure 6-9 was generated with latitude –90-90, radius 0.75-0.95, longitude –60-60.

Visualization

Volume renderings were done in ResView 3.2 (Figures 6-1, 6-4, 6-5, 6-6, 6-10, 6-11, 6-12). Extracted volumes were visualized in Amira (6-2, 6-3, 6-6, 6-7, 6-8).

1. Ewald AJ, McBride H, Reddington M, Fraser SE, Kerschmann R: **Surface imaging microscopy, an automated method for visualizing whole embryo samples in three dimensions at high resolution**. *Dev Dyn* 2002, **225**:369-375.
2. Sive HL, Grainger RM, Harland RH: *Early Development of Xenopus Laevis: A Laboratory Manual*, First edn. Cold Spring Harbor: Cold Spring Harbor Laboratory Press; 2000.
3. Nieuwkoop PD, Faber J (eds.): *Normal Table of Xenopus laevis (Daudin)*, 2nd edn. New York: Garland Publishing, Inc.; 1994.
4. Wallingford JB, Fraser SE, Harland RM: **Convergent extension: the molecular control of polarized cell movement during embryonic development**. *Dev Cell* 2002, **2**:695-706.
5. Keller R: **Shaping the vertebrate body plan by polarized embryonic cell movements**. *Science* 2002, **298**:1950-1954.
6. Keller R, Davidson L, Edlund A, Elul T, Ezin M, Shook D, Skoglund P: **Mechanisms of convergence and extension by cell intercalation**. *Philos Trans R Soc Lond B Biol Sci* 2000, **355**:897-922.
7. Ibrahim H, Winklbauer R: **Mechanisms of mesendoderm internalization in the Xenopus gastrula: lessons from the ventral side**. *Dev Biol* 2001, **240**:108-122.
8. Wacker S, Grimm K, Joos T, Winklbauer R: **Development and control of tissue separation at gastrulation in Xenopus**. *Dev Biol* 2000, **224**:428-439.
9. Winklbauer R, Medina A, Swain RK, Steinbeisser H: **Frizzled-7 signalling controls tissue separation during Xenopus gastrulation**. *Nature* 2001, **413**:856-860.
10. Keller RE: **Vital dye mapping of the gastrula and neurula of Xenopus laevis. II. Prospective areas and morphogenetic movements of the deep layer**. *Dev Biol* 1976, **51**:118-137.
11. Keller RE: **Vital dye mapping of the gastrula and neurula of Xenopus laevis. I. Prospective areas and morphogenetic movements of the superficial layer**. *Dev Biol* 1975, **42**:222-241.
12. Shih J, Keller R: **Patterns of cell motility in the organizer and dorsal mesoderm of Xenopus laevis**. *Development* 1992, **116**:915-930.
13. Davidson LA, Hoffstrom BG, Keller R, DeSimone DW: **Mesendoderm extension and mantle closure in Xenopus laevis gastrulation: combined roles for integrin alpha(5)beta(1), fibronectin, and tissue geometry**. *Dev Biol* 2002, **242**:109-129.
14. Sokol SY: **Analysis of Dishevelled signalling pathways during Xenopus development**. *Curr Biol* 1996, **6**:1456-1467.
15. Sokol SY, Klingensmith J, Perrimon N, Itoh K: **Dorsalizing and neuralizing properties of Xdsh, a maternally expressed Xenopus homolog of dishevelled**. *Development* 1995, **121**:3487.

16. Wallingford JB, Rowning BA, Vogeli KM, Rothbacher U, Fraser SE, Harland RM: **Dishevelled controls cell polarity during Xenopus gastrulation**. *Nature* 2000, **405**:81-85.
17. Rothbacher U, Laurent MN, Deardorff MA, Klein PS, Cho KW, Fraser SE: **Dishevelled phosphorylation, subcellular localization and multimerization regulate its role in early embryogenesis**. *Embo J* 2000, **19**:1010-1022.

Figure 6-1: Surface Imaging Microscopy: Surface imaging microscopy enables conversion of fixed frog embryos into high resolution digital datasets. Briefly, the frog embryo is fixed, labeled with Resolution Standard Staiin (Resolution Sciences Corporation, Corte Madera), dehydrated in ethanol, then embedded in Resolution Standard Embedding Polymer (Resolution Sciences Corporation, Corte Madera), and mounted onto the motorized translation stage (TS). This motorized stage brings the sample into the field of view of an objective lens, then draws the sample over a diamond knife to remove a thin section, then brings the freshly cut blockface of the sample back into the field of view of an objective lens. For more details see Chapter 5.

Figure 6-2: Comparison of Confocal and Surface Imaging Microscopy: Two different frog embryos were imaged with either confocal laser scanning microscopy (A) or surface imaging microscopy (B). Surface imaging microscopy provided higher contrast, more uniform imaging, and better through plane resolution. For more details see Chapter 5.

Figure 6-3: Frog Gastrulation Coordinate System: Two landmarks were selected to define a standard coordinate system for all frog gastrulae. Datasets were downsampled sixfold, and three orthogonal views through the dataset were presented to the user (A). The user then iteratively selected points until satisfied that the center of the blastopore had been identified. This point then defined the south pole of the embryo. To define the prime meridian, the program then

presented a range of sections perpendicular to the north pole–south pole axis, and presented these sections to the user. The user then identified the center of the dorsal lip of the blastopore. For more details see Appendix 2.

Figure 6-4: Digital Stage Series of Gastrulation: Four views are presented of each of six different datasets from frog gastrulae. In the first row is a volume rendering of each embryo taken from the perspective of a mid-saggital section. The second row provides a view of the outside surface of the vegetal hemisphere. The third row depicts a mid-saggital section through the dorsal midline of each embryo. Finally the bottom row shows a surface rendering of the surface of the two major cavities of the frog gastrulae: the blastocoel in purple and the archenteron in pink.

Figure 6-5: Subset of Gastrulation Series: Four embryos were selected from the digital frog gastrulation series for more detailed analysis. The same embryos are used in Figure 6-7, 6-8, 6-9 and are preserved in the same order.

Figure 6-6: Schematic of Digital Manipulations: Each of the embryo datasets from 6-5 were subjected to a three different manipulations to visualize three different morphogenetic processes. Two different volumes were extracted from the datasets. The first was a region from the south pole to the equator, with longitudinal extent ranging from +60° to –60° from the dorsal midline. When viewed from above this volume allowed us to examine the planar arrangement of

cells within epithelial sheets. When examined from edge on this same volume enabled us to view the bottle cells, the archenteron, and the interface between tissue layers. As a complementary volume we examined the entire dorsal length of the embryo, from north pole to south pole, at a longitudinal extent of +60° to –60° from the dorsal midline. When viewed from below this yielded a very useful perspective on the leading edge of the mesendoderm.

Figure 6-7: Archenteron Formation and Tissue Separation: Volumes were extracted from the series of embryos depicted in Figure 6-5 to visualize the development of tissue separation and the formation and elongation of the archenteron. Both A-D and E-H represent developmental series through the same embryos; A-D shows the 2D section at that point in the volume, whereas E-H shows the 3D volume. The tissue separation line known as Brachet's Cleft is clearly visible in each volume and its posterior limit is highlighted with a black arrow. It is worth noting that it has advanced nearly to the dorsal lip prior to involution. The arrangement of bottle cells is clearly visible in 6-7A as the dorsal lip of the blastopore first forms. The development of the archenteron progresses through sequential elongation of the archenteron (6-7B, 6-7C), followed by an inflation or expansion of the cavity (6-7D).

Figure 6-8: Vegetal Alignment Zone: The closure of the blastopore has been has been proposed to be dependent on circumferentially organized hoops of medio-laterally aligned cells, concentric with the blastopore (reviewed in [6]).

This arrangement of cells has been observed in explanted tissues [12], but not in whole embryos. To test whether we observe these cell arrangements, we selected a plane of section within the dorsal marginal zone just below Brachet's cleft (A-D) and examined the planar arrangement of cells within that layer (E-H). At early gastrula stages (E), the cells are predominantly round and display no obvious medio-lateral (left-right in panels E-H) polarity. As gastrulation proceeds more cells become polarized in the medio-lateral direction and this arrangement of cells spreads towards the anterior (top of panel) direction.

Figure 6-9: Mesendoderm Extension: The mesendoderm migrates/extends on the roof of the blastocoel at a similar time to other morphogenetic processes of gastrulation. We selected a volume along the entire dorsal length of the embryo, from north pole to south pole, at a longitudinal extent of +60° to –60° from the dorsal midline. When viewed from the perspective of the inside of the embryo looking out this volume clearly presents the leading edge of the mesendoderm (black arrows) moving along the roof of the blastocoel (faint areas). The roof of the blastocoel is thinner than surrounding tissues at these stages and so appears more transparent.

Figure 6-10: Xdd1 embryos at Stage 10.5: Embryos were injected with RNA encoding a mutant form of Dishevelled that disrupted Wnt signaling activity, Xdd1 [17]. Embryos were imaged with surface imaging microscopy at approximately

stage 10.5. No major differences were observed between control embryos and injected embryos.

Figure 6-11: Xdd1 embryos at Stage 12: Embryos were injected with RNA encoding a mutant form of Dishevelled that disrupted Wnt signaling activity, Xdd1 [17]. Embryos were imaged with surface imaging microscopy at approximately stage 12. Several differences are apparent between control and treated embryos. In Xdd1 injected embryos the archenteron is shorter and has a smaller volume, while the blastocoel has a larger volume. The thickness of the dorsal marginal zone is also greater.

Figure 6-12: Morphometrics of Frog Gastrulation: We became interested in the coupling of different morphogenetic cell movements during gastrulation and devised a series of metrics to evaluate the degree of success of different processes in control and treated embryos. Embryos will first be photographed from the vegetal side (Panel A) to establish the degree of blastopore closure. Then the length to width ratio of the developing notochord will be calculated (Panel B). Finally the embryos will be bisected and the length of the archenteron will be normalized to the diameter of the embryo. Each of these measurements is converted to a unitless ratio to ease comparison between embryos of different sizes. Comparisons will be made between wildtype embryos to establish the normal degree of coupling of the different processes during gastrulation and

comparisons will be made between normal and experimental conditions to test which processes are obligately coupled.

Fixed Frog Embryo

Digital Frog Embryo

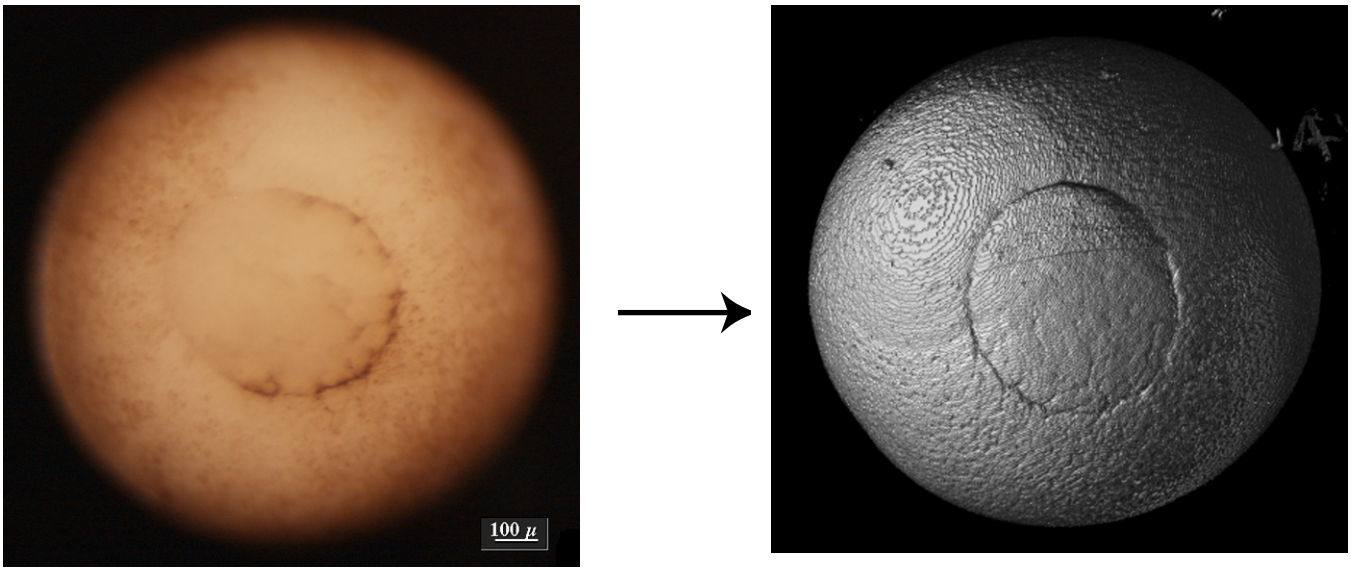

A

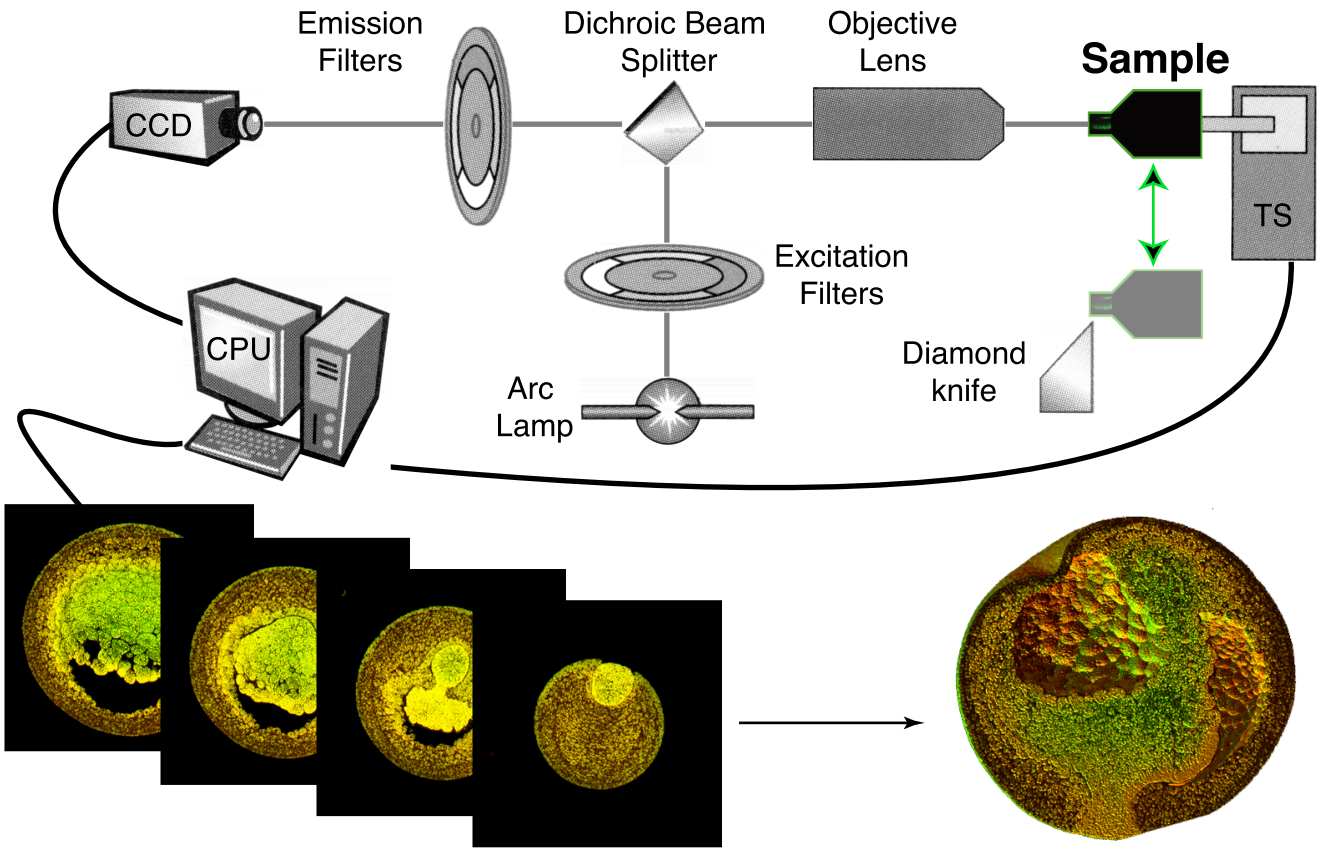

B

2D Raw Images

3D Reconstruction

A

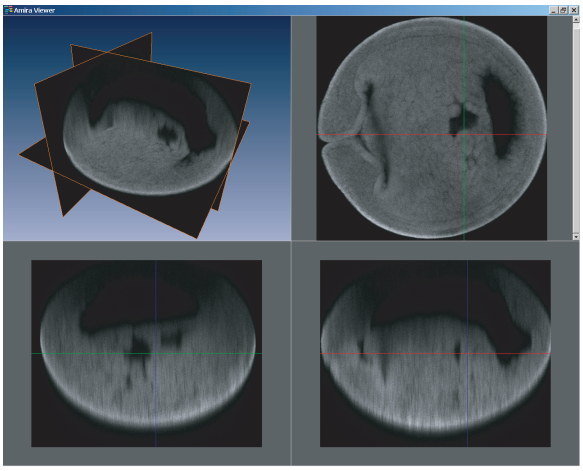

Confocal
Frog
Dataset

B

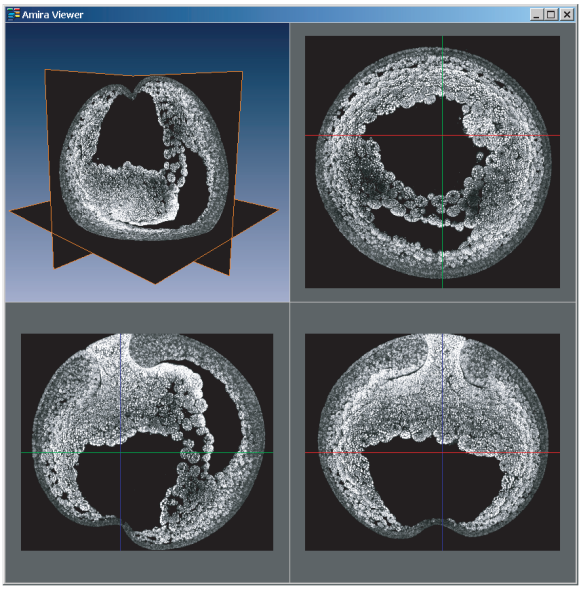

SIM
Frog
Dataset

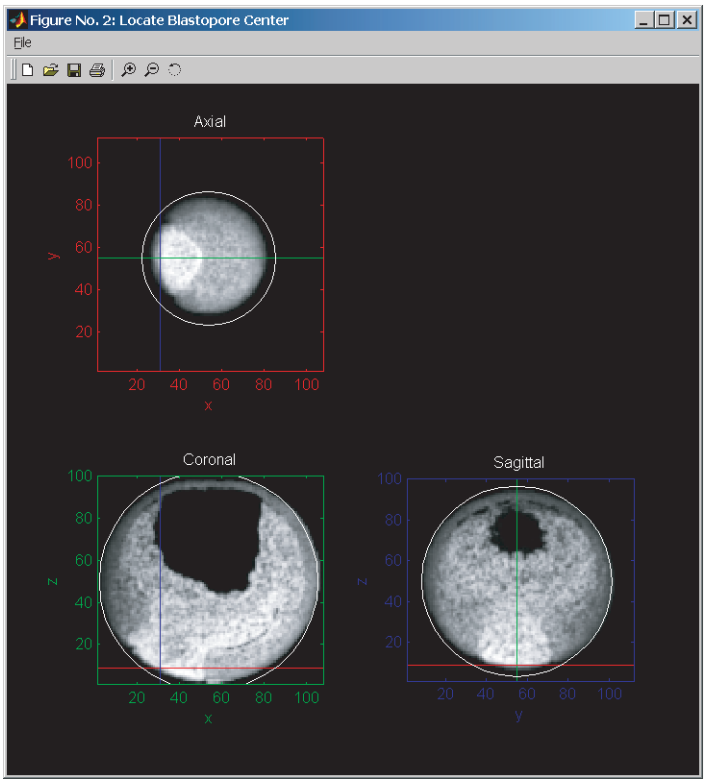
Figure No. 2: Locate Blastopore Center
File
Axial
Coronal
Sagittal

A

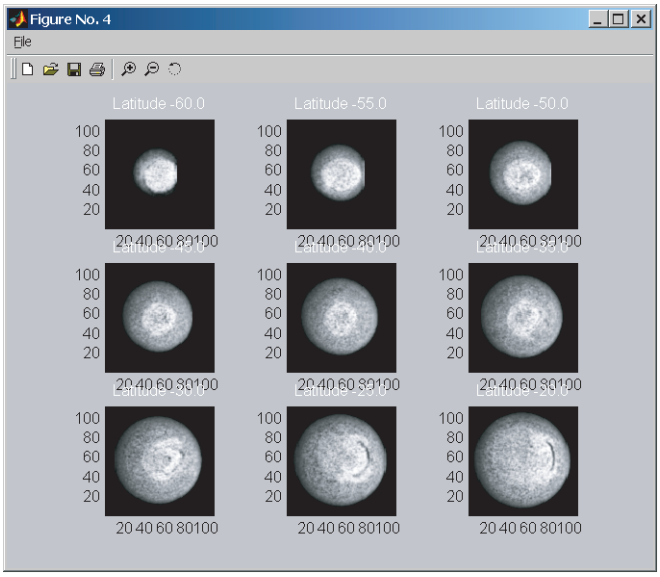
Figure No. 4
File
Latitude -60.0
Latitude -55.0
Latitude -50.0

B

A Four Dimensional View of Normal Xenopus Gastrulation

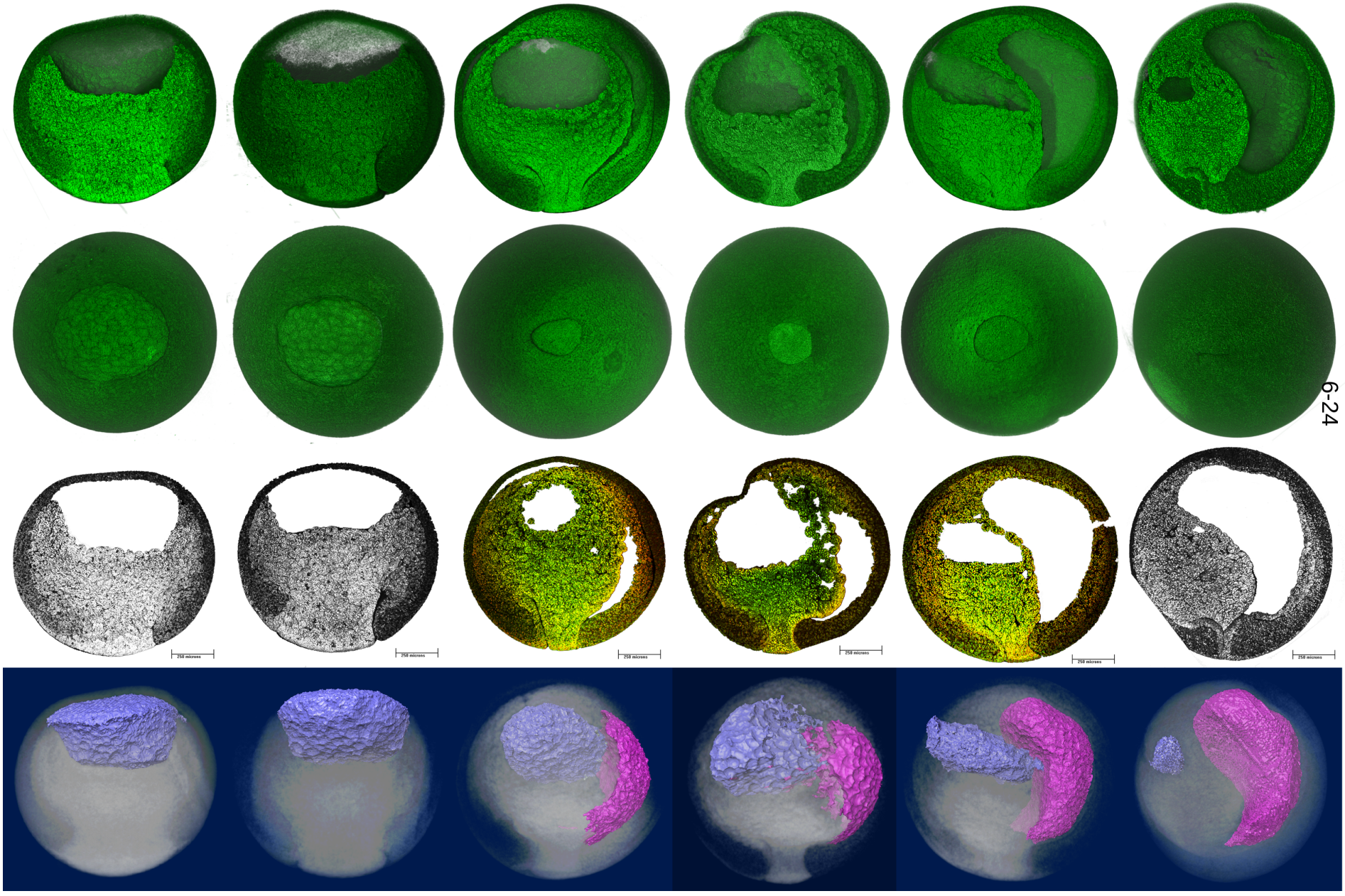

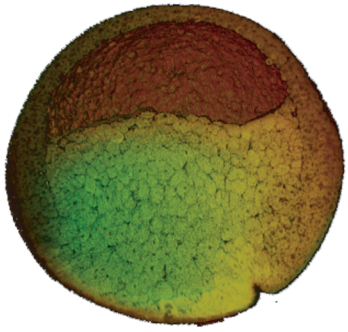

A

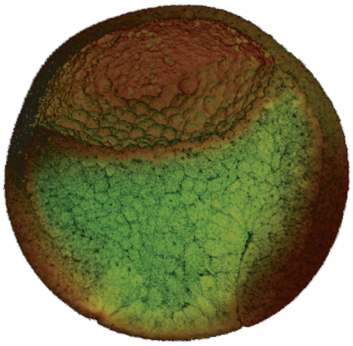

B

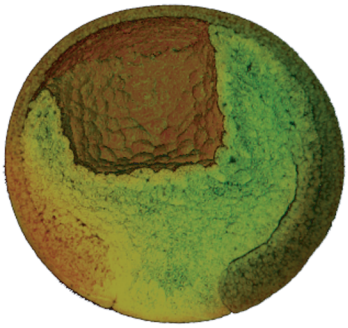

C

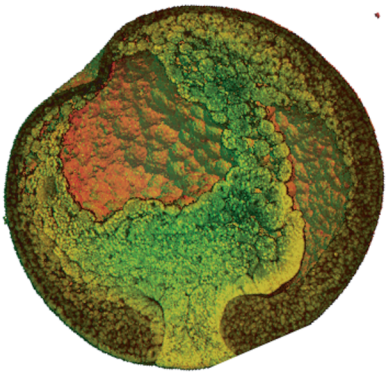

D

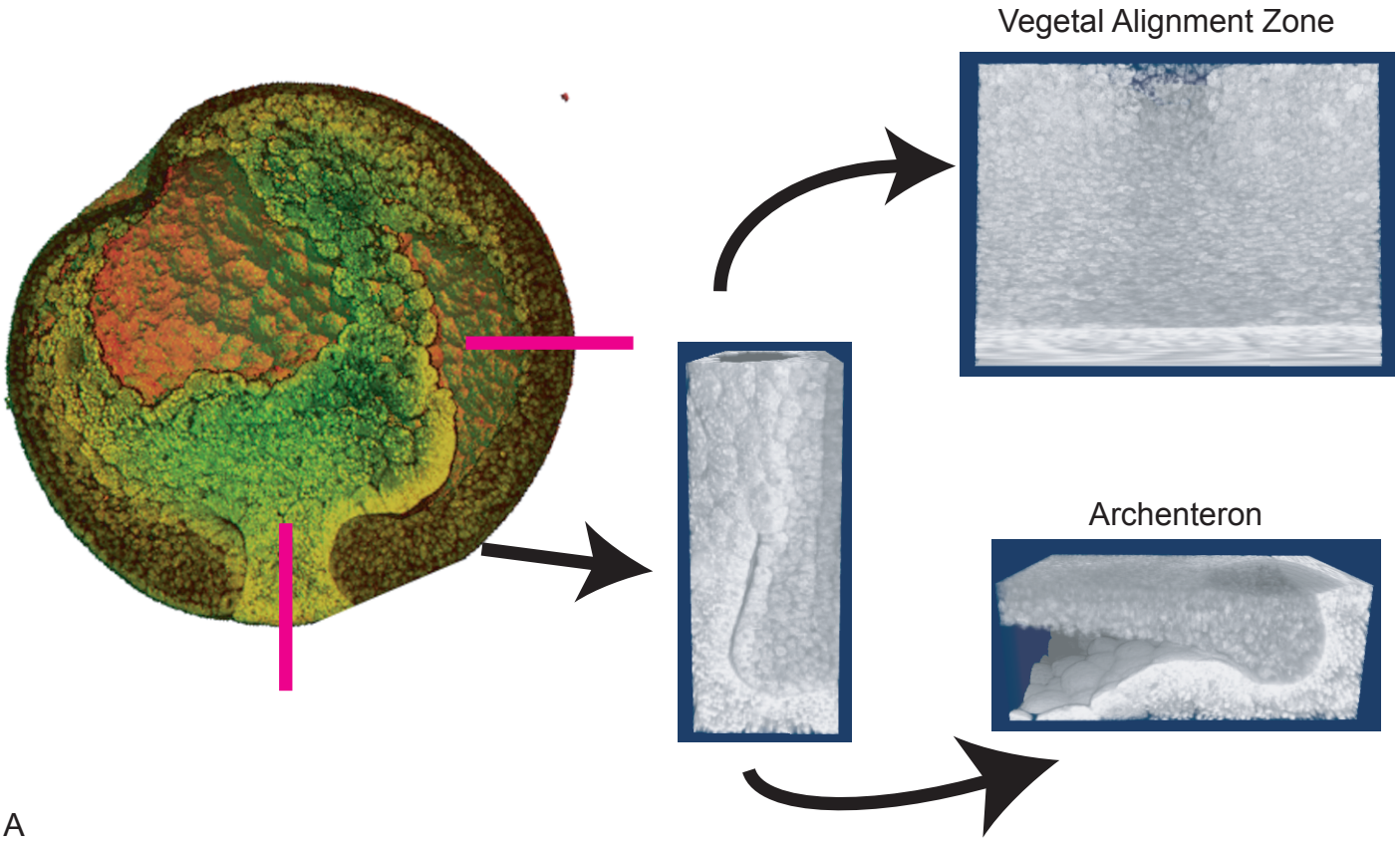
Vegetal Alignment Zone
Archenteron

A

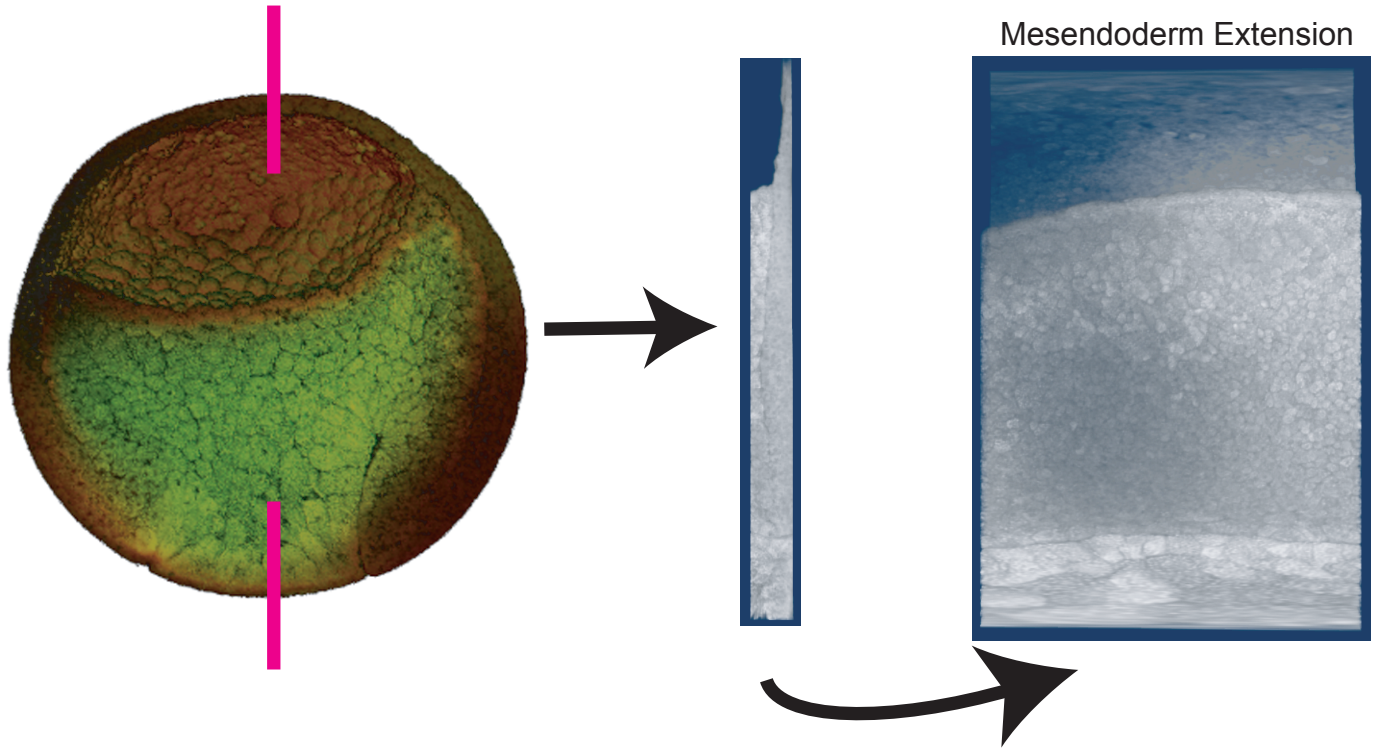
Mesendoderm Extension

B

A 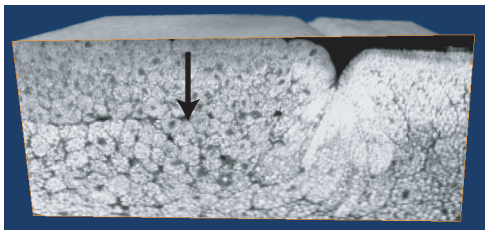

B 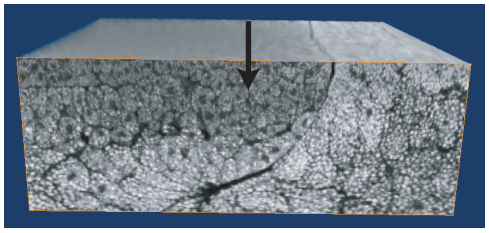

C 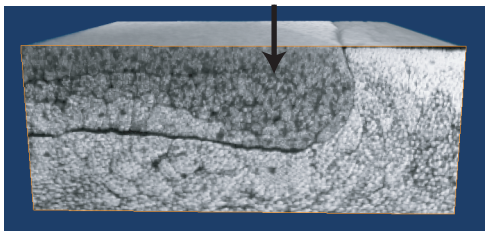

D 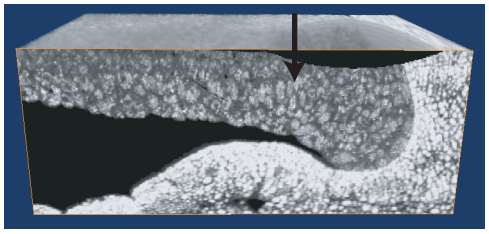

D 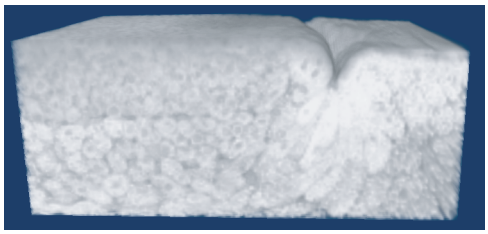

E 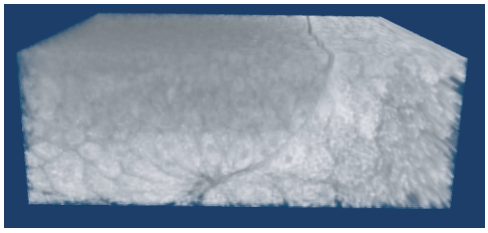

F 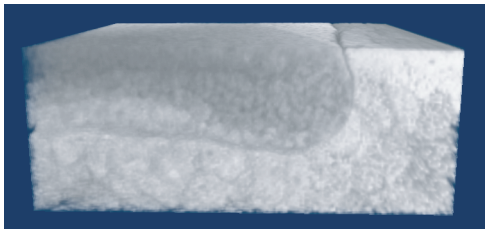

G 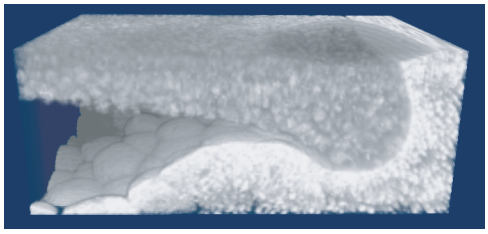

A

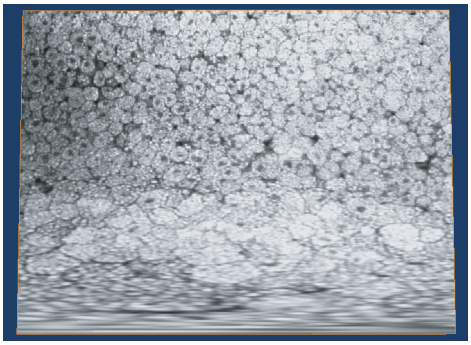

D

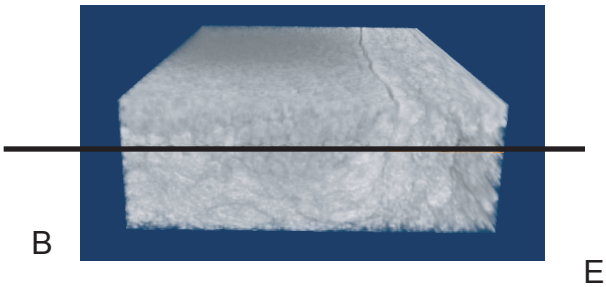

B

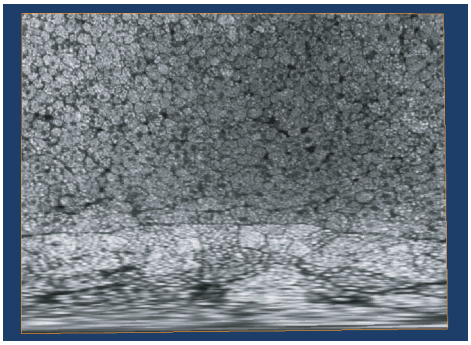

E

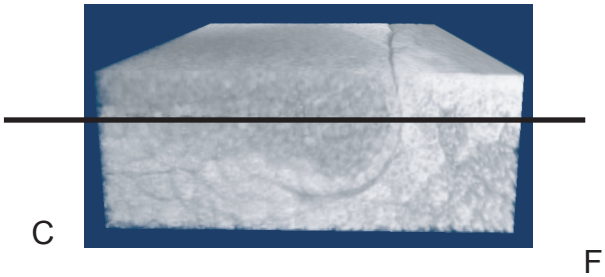

C

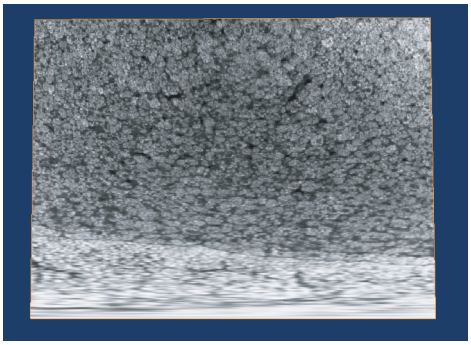

F

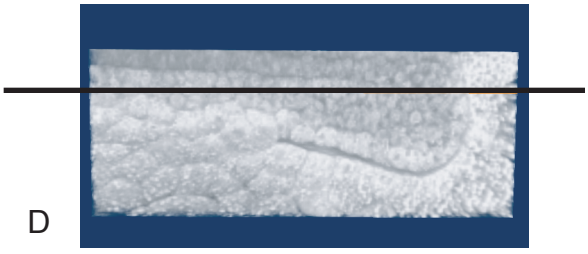

D

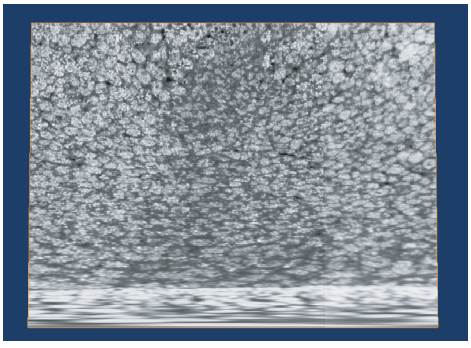

G

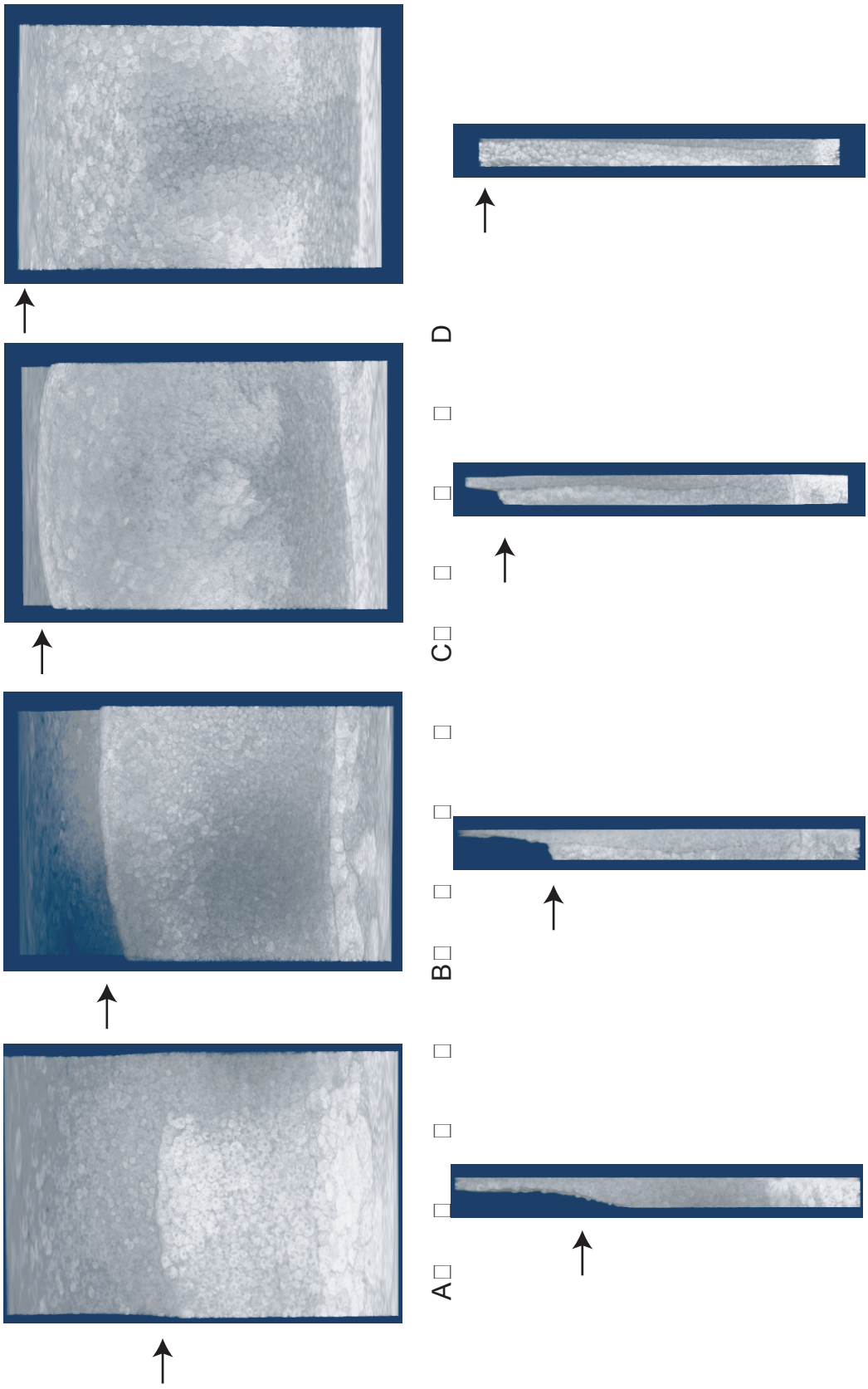
D
C
B
A

Control Stage 10.5 Frog Embryos

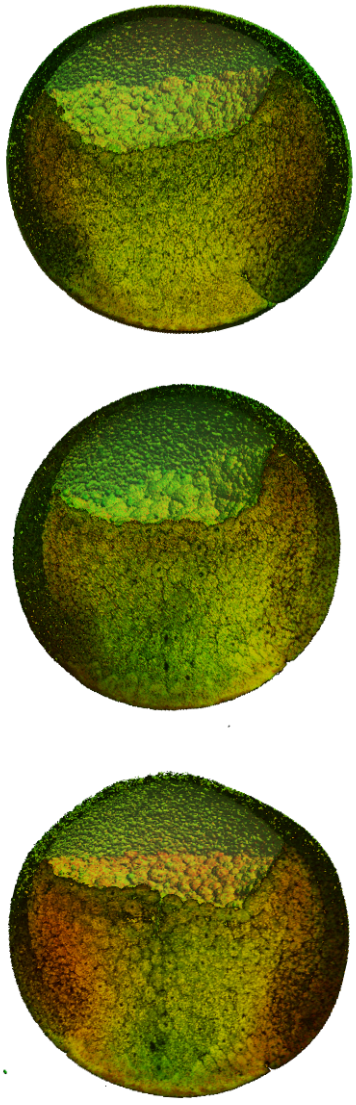

Xdd1 Injected Stage 10.5 Frog Embryos

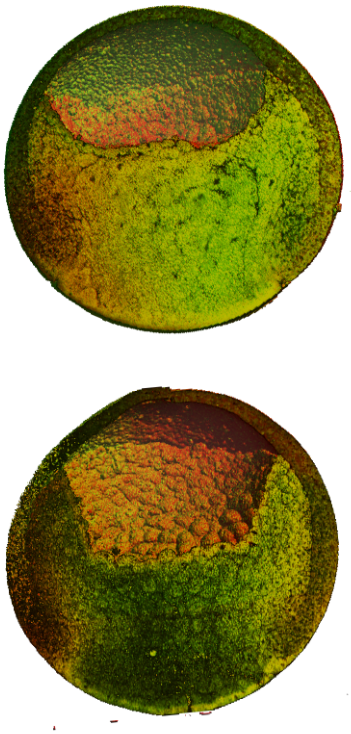

Control Stage 12 Frog Embryos

Xdd1 Injected Stage 12 Frog Embryos

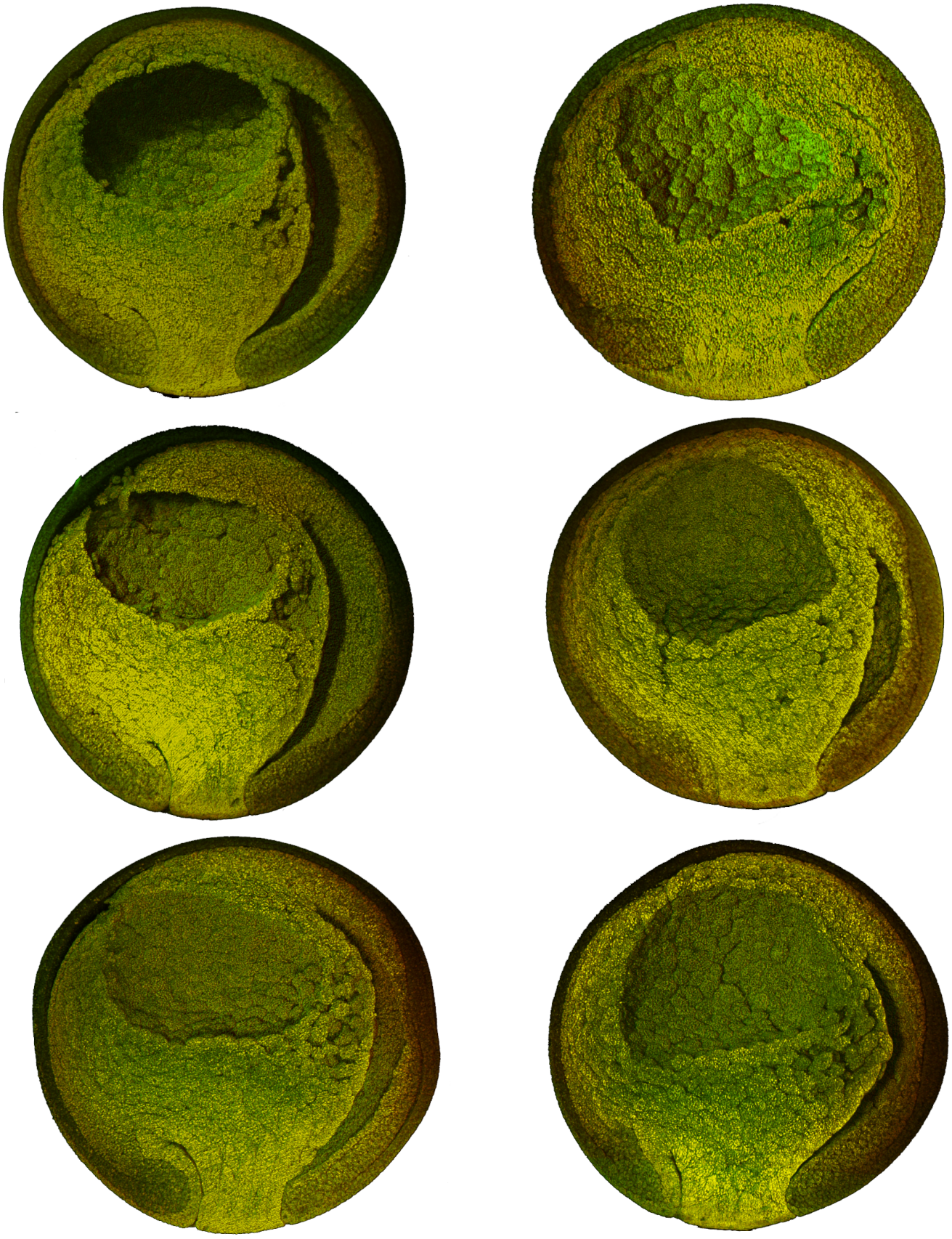

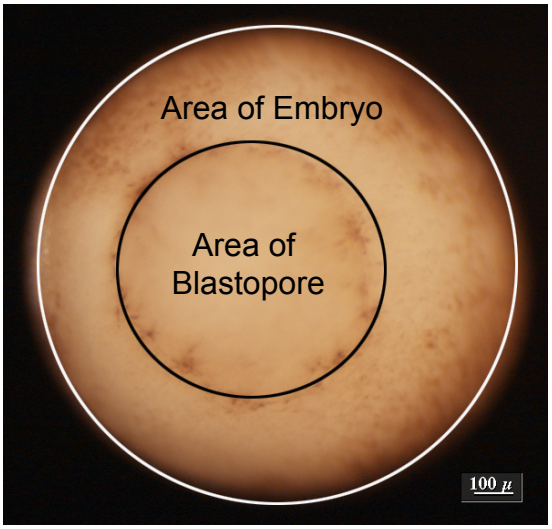
Area of Embryo
Area of
Blastopore
100 µ

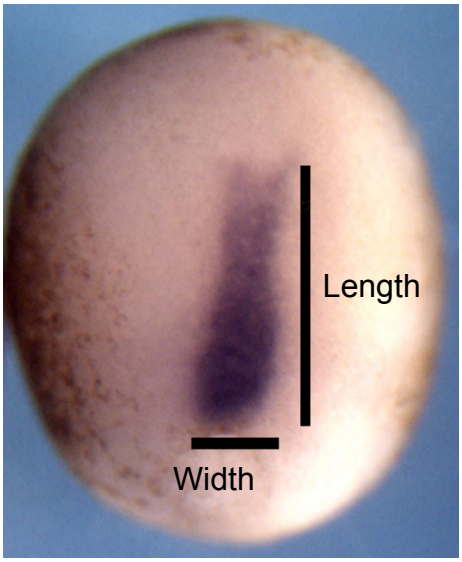
Length
Width

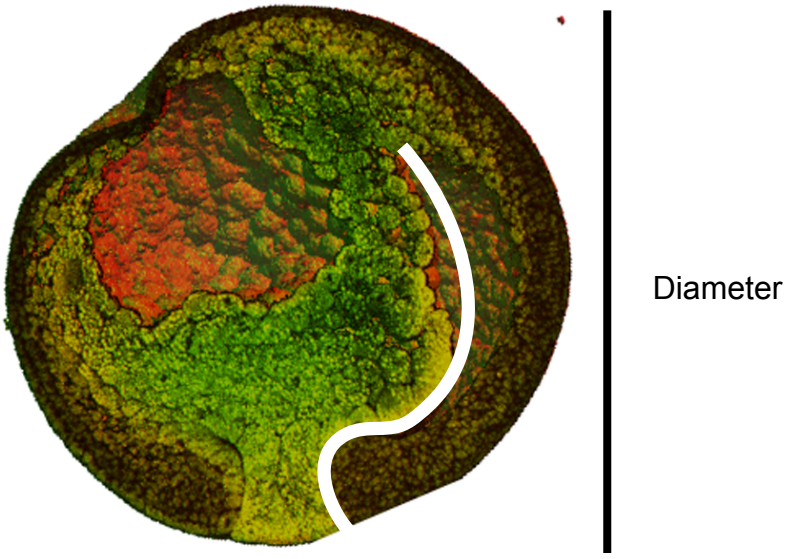
Diameter
Archenteron Length